An adaptive least angle regression method for uncertainty quantification in FDTD computation

Runze Hu, Fumie Costen, *Senior Member, IEEE*, Vikass Monebhurrun, *Senior Member, IEEE*, Ryutaro Himeno, Hideo Yokota

***Abstract*—The non-intrusive polynomial chaos (NIPC) expansion method is used to quantify the uncertainty of a stochastic system. It potentially reduces the number of numerical simulations in modelling process, thus improving efficiency, whilst ensuring accuracy. However, the number of polynomial bases grows substantially with the increase of random parameters, which may render the technique ineffective due to the excessive computational resources. To address such problems, methods based on the sparse strategy such as the least angle regression (LARS) method with hyperbolic index sets can be used. This paper presents the first work to improve the accuracy of the original LARS method for uncertainty quantification (UQ). We propose an adaptive LARS method in order to quantify the uncertainty of the results from the numerical simulations with higher accuracy than the original LARS method. The proposed method outperforms the original LARS method in terms of accuracy and stability. The L2 regularisation scheme further reduces the number of input samples while maintaining the accuracy of the LARS method.**

***Index Terms*—Non-intrusive polynomial chaos (NIPC) expansion, least angle regression (LARS), uncertainty quantification (UQ), finite difference time domain (FDTD), Debye media**

I. Introduction

Benefiting from the rapid development of communication technology, wireless communication devices such as mobile phones [1], [2] have grown in popularity, raising concern about the potential dangers of exposure to electromagnetic radiation [3], [4]. Tissues in the immediate vicinity absorb the radio frequency (RF) energy emitted from the wireless devices, which may potentially be hazardous [5]. To evaluate the energy absorption when the human body is exposed to an RF electromagnetic field, the specific absorption rate (SAR) [6], [7] is measured using a standard dosimetric test facility. However, since the SAR test is expensive and time-consuming, the use of electromagnetic simulation to model the RF energy exposure is a preferred alternative.

The finite difference time domain (FDTD) [8], [9] method has a powerful and robust performance in modeling inhomogeneous materials and the simulation of wideband antennae, which makes it a suitable method for bioelectromagnetic simulations. To explore the propagation of the electromagnetic waves in human body, a digital human phantom (DHP) is introduced into the FDTD space. One of the main advantages [10] of utilising a DHP is that it allows researchers to test the electromagnetic response without exposing human body to the electromagnetic radiation.

In the FDTD calculations, the one-pole Debye model [11] is utilised to describe the complex frequency-dependent behaviour of biological tissues. Each tissue in the DHP is associated with four Debye parameters and these parameters differ between people. Such variation is taken into account by introducing uncertainty. In the numerical simulations, the Debye parameters are considered as the input parameters of the system used to determine the electromagnetic response of the human body. The uncertainty of these input parameters can be described by their probabilistic description [12]. However, uncertainty also exists in the system response, due to the propagation of the randomness of the input parameters.

This paper focuses on the uncertainty quantification (UQ) of the FDTD method. The traditional approach for UQ is the Monte Carlo method (MCM) [13], [14], yet this technique requires a large number of simulations resulting in computational inefficiency. Although methods such as the Latin Hypercube sampling (LHS) method [15] and the Markov Chain Monte Carlo (MCMC) method [16] are capable of speeding up the convergence rate of the MCM method, the applications of MCM are very limited because the computational requirements are still excessive.

The non-intrusive polynomial chaos (NIPC) expansion method [17], [18] is one of the most frequently used methods for UQ as an alternative to MCM. We obtain the coefficients of the NIPC method mainly from the Galerkin projection method [19] or the regression method [20]. Nevertheless, both methods are prone to the *curse of dimensionality*, whereby the number of calculations grows with the increase of the number of input parameters, leading to the rise of the computational cost. A solution to this problem was proposed in [18] wherein each parameter is considered one at a time.

To circumvent the *curse of dimensionality*, a truncation scheme known as the hyperbolic polynomial chaos expansion [21] is applied in this work. This reduces the number of polynomial bases, based on the sparsity-of-effects principle. When we have multiple variables, the higher-order Hermite polynomials may be less significant than the lower-order ones [22]. Thus, the sparse polynomial chaos (PC) expansion can be built by discarding less important polynomial bases without

R. Hu and F. Costen are with the School of Electrical and Electronic Engineering, The University of Manchester, U.K. (email: fumie.costen@manchester.ac.uk).

V. Monebhurrun is with the EXPOSE/PIEM/GEEPS, CentraleSupelec, 11 rue Joliot Curie Plateau de Moulon, Gif sur Yvette 91192, France (e-mail: Vikass.MONEBHURRUN@centralesupelec.fr).

R. Himeno is with Head Office for Information Systems and Cybersecurity, RIKEN, Saitama, Japan.

H. Yokota and F. Costen are with the Image Processing Research Team, Centre for Advanced Photonics, RIKEN, Saitama, Japan.

Color version of the figures in this paper are available online at http://ieeexplore.ieee.org.

Additional research data supporting this publication are available from http://dx.doi.org/ repository at 10.17632/tpvrtz3w6z.1.

sacrificing accuracy. To quantify the uncertainty of the FDTD results using only significant Hermite polynomial bases, a classical model selection method, known as the least angle regression (LARS) method [21], [23], is undertaken. Given a set of possible polynomial bases, the LARS method aims to select those polynomial bases which possess high correlation with the output of the system. The LARS procedure consists of a number of iterations, each of which is concerned with the selection of the most correlated polynomial bases. A termination criterion is usually set in order to control the LARS procedure, thereby resulting in the selection of only a limited number of polynomial bases. Such features render the LARS method computationally efficient. However, the LARS method has never been applied to quantify the uncertainty of the FDTD results.

This paper proposes an adaptive LARS method for our in-house FDTD code mainly focusing on the improvement of the accuracy of the LARS method. To successfully perform the matrix inversion in the LARS method, the number of input samples must exceed the number of polynomial bases. Such a condition restricts the minimum number of input samples. However, when the condition is not met, this does not necessarily imply that the LARS method underperforms or is excessively inaccurate. To explore the relationship between the accuracy of the LARS method and the required number of input samples, the L2 regularisation scheme [24] is incorporated into the LARS method to enable the technique to function irrespective of the number of input samples. As a result, the number of input samples may be further reduced without degrading the accuracy of the LARS method. The paper is organised as follows: Section II explains the principle of the hyperbolic scheme, the LARS method and proposes the adaptive LARS method. Section III details the numerical experiments for UQ by MCM, LARS and the adaptive LARS methods. Finally, we analyse the results from these techniques and emphasise the merit of the adaptive LARS method.

II. Methodology

The hyperbolic scheme enables us to build a sparse PC expansion. The LARS and adaptive LARS methods are used to quantify the uncertainty of the FDTD results.

A. The non-intrusive polynomial chaos expansion

The NIPC method approximates the random outputs of the system using a series of orthogonal polynomials. In the NIPC method, quantifying the uncertainty of a system is equivalent to the calculation of the coefficients of polynomial bases [25]. The polynomial basis is defined as $\psi_{\alpha_1\alpha_2\cdots\alpha_{\mathcal{K}}}(\xi_1,\xi_2,\cdots,\xi_{\mathcal{K}})$, where $\alpha_1\alpha_2\cdots\alpha_{\mathcal{K}}$ is the index of the polynomial basis, and $\xi_1,\xi_2,\cdots,\xi_{\mathcal{K}}$ are $\mathcal{K}$ variables. In this paper, each variable ξ_k represents a certain Debye parameter of interest of a certain tissue and we observe the electric field $\boldsymbol{E}$ in the FDTD simulations. The highest order of the polynomial basis in a PC expansion is denoted as $r \in [1,+\infty)$. r is set to a certain finite value so that the PC expansion is truncated from the infinite PC expansion. In this case, α_k satisfies

$$\sum_{k=1}^{\mathcal{K}} \alpha_k \leq r, \alpha_k \geq 0 \tag{1}$$

and the total number of polynomial bases in the NIPC expansion is

$$\mathcal{L} = \frac{(\mathcal{K}+r)!}{\mathcal{K}!r!}. \tag{2}$$

For example, in the case of $r = 2$ and $\mathcal{K} = 3$, the number of polynomial bases in the PC expansion is $\mathcal{L} = 10$ in (2), and the Hermite polynomials $\psi_{\alpha_1\alpha_2\alpha_3}(\xi_1,\xi_2,\xi_3)$ are shown in Table I.

Hermite polynomials	The order of ψ
$\psi_{000}(\xi_1,\xi_2,\xi_3) = \psi_0(\xi_1)\psi_0(\xi_2)\psi_0(\xi_3) = 1$	0
$\psi_{100}(\xi_1,\xi_2,\xi_3) = \psi_1(\xi_1)\psi_0(\xi_2)\psi_0(\xi_3) = \xi_1$	1
$\psi_{010}(\xi_1,\xi_2,\xi_3) = \psi_0(\xi_1)\psi_1(\xi_2)\psi_0(\xi_3) = \xi_2$	
$\psi_{001}(\xi_1,\xi_2,\xi_3) = \psi_0(\xi_1)\psi_0(\xi_2)\psi_1(\xi_3) = \xi_3$	
$\psi_{200}(\xi_1,\xi_2,\xi_3) = \psi_2(\xi_1)\psi_0(\xi_2)\psi_0(\xi_3) = \xi_1^2 - 1$	2
$\psi_{020}(\xi_1,\xi_2,\xi_3) = \psi_0(\xi_1)\psi_2(\xi_2)\psi_0(\xi_3) = \xi_2^2 - 1$	
$\psi_{002}(\xi_1,\xi_2,\xi_3) = \psi_0(\xi_1)\psi_0(\xi_2)\psi_2(\xi_3) = \xi_3^2 - 1$	
$\psi_{110}(\xi_1,\xi_2,\xi_3) = \psi_1(\xi_1)\psi_1(\xi_2)\psi_0(\xi_3) = \xi_1\xi_2$	
$\psi_{101}(\xi_1,\xi_2,\xi_3) = \psi_1(\xi_1)\psi_0(\xi_2)\psi_1(\xi_3) = \xi_1\xi_3$	
$\psi_{011}(\xi_1,\xi_2,\xi_3) = \psi_0(\xi_1)\psi_1(\xi_2)\psi_1(\xi_3) = \xi_2\xi_3$	

TABLE I
THE HERMITE POLYNOMIALS $\psi_{\alpha_1\alpha_2\alpha_3}(\xi_1,\xi_2,\xi_3)$ AND THE CORRESPONDING ORDERS

B. The hyperbolic scheme for PC expansion

The hyperbolic scheme restricts the combination of $\alpha_1\alpha_2...\alpha_{\mathcal{K}}$ in the PC expansion to satisfy

$$\left(\sum_{k=1}^{\mathcal{K}} \alpha_k^q\right)^{\frac{1}{q}} \leq r \tag{3}$$

for $0 < q \leq 1$, and thus the number of polynomial bases in the PC expansion in (2) can be reduced, based on q-quasi-norm [21]. When q equals 1, (3) becomes the usual truncation scheme as shown in (1). When we set q to 0.4, the number of retained polynomial bases is reduced to 7 based on (3). The retained polynomial bases are presented in Table II for $q = 1$ and $q = 0.4$.

q	$\alpha_1\alpha_2\alpha_3$ in $\psi_{\alpha_1\alpha_2\alpha_3}(\xi_1,\xi_2,\xi_3)$
1	000, 100, 010, 001, 200, 020, 002, 110, 101, 011
0.4	000, 100, 010, 001, 200, 020, 002

TABLE II
RETAINED POLYNOMIAL BASES WHEN $q = 1$ AND $q = 0.4$

C. The least angle regression

1) The linear regression model:
Assuming there are $\mathcal{K}$ Debye parameters of interest and $\mathcal{M}$ sets of input samples, we define the vector $\boldsymbol{\xi} = \{\xi_1,\xi_2,\cdots,\xi_{\mathcal{K}}\}$ as the combination of these Debye parameters, and $\boldsymbol{\xi}^{(m)}$ as the m-th $\boldsymbol{\xi}$ for $1 \leq m \leq \mathcal{M}$. The LARS method is a classic model-selection method [21]. It aims to

select the polynomial bases ψ that highly correlate with the output of the linear regression model of

$$\mathcal{T}(\boldsymbol{\xi}^{(m)}) = \sum_{l=1}^{\mathcal{L}} a_{\boldsymbol{\alpha}_l} \psi_{\boldsymbol{\alpha}_l}(\boldsymbol{\xi}^{(m)}), \tag{4}$$

where $\mathcal{T}(\boldsymbol{\xi}^{(m)})$ is the predicted value of $|\boldsymbol{E}|^2$ for $\boldsymbol{\xi}^{(m)}$, the polynomial term $a_{\boldsymbol{\alpha}_l}\psi_{\boldsymbol{\alpha}_l}(\boldsymbol{\xi}^{(m)})$ is called a predictor of $\mathcal{T}(\boldsymbol{\xi}^{(m)})$, $\boldsymbol{\alpha}_l$ indicates the index of the l-th ψ, and a is the coefficient of ψ.

Let $\boldsymbol{a}$ be a vector which consists of $\mathcal{L}$ coefficients as in $\boldsymbol{a} = \{a_{\boldsymbol{\alpha}_1}, \cdots, a_{\boldsymbol{\alpha}_\mathcal{L}}\}^T$, $\widehat{\mathcal{T}}(\boldsymbol{\xi}^{(m)})$ be the current LARS update of $\mathcal{T}(\boldsymbol{\xi}^{(m)})$ and the vector $\widehat{\boldsymbol{\mathcal{T}}} = \{\widehat{\mathcal{T}}(\boldsymbol{\xi}^{(1)}), \cdots, \widehat{\mathcal{T}}(\boldsymbol{\xi}^{(\mathcal{M})})\}^T$. The matrix $\boldsymbol{\Psi} = (\psi_{\boldsymbol{\alpha}_l}(\boldsymbol{\xi}^{(m)}), m = 1 \sim \mathcal{M}, l = 1 \sim \mathcal{L})$ formed by the polynomial bases is presented as

$$\boldsymbol{\Psi} = \begin{bmatrix} \psi_{\boldsymbol{\alpha}_1}(\boldsymbol{\xi}^{(1)}) & \psi_{\boldsymbol{\alpha}_2}(\boldsymbol{\xi}^{(1)}) & \cdots & \psi_{\boldsymbol{\alpha}_\mathcal{L}}(\boldsymbol{\xi}^{(1)}) \\ \psi_{\boldsymbol{\alpha}_1}(\boldsymbol{\xi}^{(2)}) & \psi_{\boldsymbol{\alpha}_2}(\boldsymbol{\xi}^{(2)}) & \cdots & \psi_{\boldsymbol{\alpha}_\mathcal{L}}(\boldsymbol{\xi}^{(2)}) \\ \vdots & \vdots & \ddots & \vdots \\ \psi_{\boldsymbol{\alpha}_1}(\boldsymbol{\xi}^{(\mathcal{M})}) & \psi_{\boldsymbol{\alpha}_2}(\boldsymbol{\xi}^{(\mathcal{M})}) & \cdots & \psi_{\boldsymbol{\alpha}_\mathcal{L}}(\boldsymbol{\xi}^{(\mathcal{M})}) \end{bmatrix}.$$

2) The LARS iteration:

At the start of the LARS method, $\boldsymbol{a}$ is initialised to $\boldsymbol{0}$. Let $\boldsymbol{\mathcal{C}} = \{\mathcal{C}_1, \mathcal{C}_2, \cdots, \mathcal{C}_\mathcal{L}\}^T$ be the vector of the correlation between ψ and $(\boldsymbol{\mathcal{E}} - \widehat{\boldsymbol{\mathcal{T}}})$ calculated as in

$$\boldsymbol{\mathcal{C}} = \boldsymbol{\Psi}^T(\boldsymbol{\mathcal{E}} - \widehat{\boldsymbol{\mathcal{T}}}), \tag{5}$$

where $\boldsymbol{\mathcal{E}} = \{|\boldsymbol{E}_1|^2, \cdots, |\boldsymbol{E}_\mathcal{M}|^2\}^T$ is a vector of the $\mathcal{M}$ $|\boldsymbol{E}|^2$ obtained from the FDTD simulations, and $|\boldsymbol{E}_m|$ is $|\boldsymbol{E}|$ when $\boldsymbol{\xi}^{(m)}$ is used for the FDTD computation and the difference between $\boldsymbol{\mathcal{E}}$ and $\widehat{\boldsymbol{\mathcal{T}}}$ is called the residual vector. The value of $\widehat{\mathcal{T}}(\boldsymbol{\xi}^{(m)})$ is also initialised to zero at the start of LARS method. Each element in $\boldsymbol{\mathcal{C}}$ such as $\mathcal{C}_l$ refers to the correlation between $\psi_{\boldsymbol{\alpha}_l}$ and the residual vector. When $\widetilde{k}$ satisfies

$$|\mathcal{C}_{\widetilde{k}}| = \max_{1 \le l \le \mathcal{L}} |\mathcal{C}_l|, \tag{6}$$

the $\psi_{\boldsymbol{\alpha}_{\widetilde{k}}}$, which has the highest correlation with the residual vector, and its corresponding coefficient $a_{\boldsymbol{\alpha}_{\widetilde{k}}}$ are chosen as a predictor of $\mathcal{T}(\boldsymbol{\xi})$. We put the chosen $a_{\boldsymbol{\alpha}_{\widetilde{k}}}\psi_{\boldsymbol{\alpha}_{\widetilde{k}}}$ into a set $\mathcal{Q}$ as in $\mathcal{Q} = \{a_{\boldsymbol{\alpha}_{\widetilde{k}}}\psi_{\boldsymbol{\alpha}_{\widetilde{k}}}\}$ and put $\widetilde{k}$ into a set $\mathcal{A}$ as in $\mathcal{A} = \{\widetilde{k}, \widetilde{k} \in [1, \mathcal{L}]\}$, where the number of elements in $\mathcal{A}$ increases with the iteration. A matrix $\hat{\boldsymbol{\Psi}}$ represents the chosen ψ as in $\hat{\boldsymbol{\Psi}} = (\psi_{\boldsymbol{\alpha}_{\widetilde{k}}}(\boldsymbol{\xi}^{(m)}), m = 1 \sim \mathcal{M}, \widetilde{k} \in [1, \mathcal{L}])$ and a vector $\hat{\boldsymbol{a}}$ indicates the coefficients of the chosen ψ as in $\hat{\boldsymbol{a}} = \{a_{\boldsymbol{\alpha}_{\widetilde{k}}}, \widetilde{k} \in [1, \mathcal{L}]\}^T$. At the first LARS iteration, for example, when $\widetilde{k} = 6$, we form $\hat{\boldsymbol{\Psi}} = \{\psi_{\boldsymbol{\alpha}_6}(\boldsymbol{\xi}^{(1)}), \cdots, \psi_{\boldsymbol{\alpha}_6}(\boldsymbol{\xi}^{(\mathcal{M})})\}^T$ from Table I and calculate $\hat{\boldsymbol{a}}$ as in

$$\hat{\boldsymbol{a}} = (\hat{\boldsymbol{\Psi}}^T\hat{\boldsymbol{\Psi}})^{-1}\hat{\boldsymbol{\Psi}}^T\boldsymbol{\mathcal{E}}. \tag{7}$$

As $\hat{\boldsymbol{a}} = \{a_{\boldsymbol{\alpha}_6}\}^T$, (7) practically calculates the value of $a_{\boldsymbol{\alpha}_6}$ and $\boldsymbol{a}$ thus becomes $\{0, \cdots, 0, a_{\boldsymbol{\alpha}_6}, 0, \cdots, 0\}^T$. $\widehat{\mathcal{T}}(\boldsymbol{\xi}^{(m)})$ is updated as in

$$\widehat{\mathcal{T}}^{(w+1)}(\boldsymbol{\xi}^{(m)}) = \widehat{\mathcal{T}}^{(w)}(\boldsymbol{\xi}^{(m)}) + \hat{\gamma}_{\widetilde{k}^{(w)}} a_{\boldsymbol{\alpha}_{\widetilde{k}^{(w)}}} \psi_{\boldsymbol{\alpha}_{\widetilde{k}^{(w)}}}, \tag{8}$$

where $\widehat{\mathcal{T}}^{(w)}(\boldsymbol{\xi}^{(m)})$ and $\widetilde{k}^{(w)}$ are $\widehat{\mathcal{T}}(\boldsymbol{\xi}^{(m)})$ and $\widetilde{k}$ at w-th LARS iteration and $\hat{\gamma}_{\widetilde{k}}$ indicates the update coefficient of the LARS method corresponding to the $\widetilde{k}$-th polynomial basis. $\hat{\gamma}_{\widetilde{k}}$ can be calculated by

$$\hat{\gamma}_{\widetilde{k}} = \min^+ \left\{ \frac{|\mathcal{C}_{\widetilde{k}}| - \mathcal{C}_{\widetilde{k}}}{A_\mathcal{A} - a_{\boldsymbol{\alpha}_{\widetilde{k}}}}, \frac{|\mathcal{C}_{\widetilde{k}}| + \mathcal{C}_{\widetilde{k}}}{A_\mathcal{A} + a_{\boldsymbol{\alpha}_{\widetilde{k}}}} \right\}, \tag{9}$$

where "$\min^+$" indicates that $\hat{\gamma}_{\widetilde{k}}$ only takes the positive minimum component in (9) and $A_\mathcal{A}$ is given by

$$A_\mathcal{A} = \left(1_\mathcal{A}^T \hat{\boldsymbol{\Psi}}^T \hat{\boldsymbol{\Psi}} 1_\mathcal{A}\right)^{-\frac{1}{2}}, \tag{10}$$

where $1_\mathcal{A}$ is a vector of 1 of length equaling the size of $\mathcal{A}$ as in $1_\mathcal{A} = \{1, 1, \cdots, 1\}^T$. When $\mathcal{A}$ includes one element $\mathcal{A} = \{6\}$, $1_\mathcal{A}$ equals $1_\mathcal{A} = \{1\}^T$. In the successive iteration, $\widetilde{k}^{(w)}$ meets (6) and $\widetilde{k}^{(w)} \neq \widetilde{k}^{(w^\dagger)}$ where $1 \le w^\dagger < w$.

Such a process of determining a predictor, adding it into $\mathcal{Q}$, and updating $\widehat{\mathcal{T}}(\boldsymbol{\xi}^{(m)})$ is called a LARS iteration. At each LARS iteration, one non-zero form of $a_{\boldsymbol{\alpha}_l}\psi_{\boldsymbol{\alpha}_l}$ is included into $\mathcal{Q}$. As a result, the number of elements in $\mathcal{Q}$ is the same as the LARS iteration number. The maximum number of the LARS iteration equals $\mathcal{L}$, in which case all ψ are incorporated in $\mathcal{Q}$.

3) The leave-one-out cross-validation method:

After each LARS iteration, we calculate $\mathcal{T}(\boldsymbol{\xi}^{(m)})$ in (4) and use the leave-one-out cross-validation (LOOCV) method [26] to evaluate the accuracy of $\mathcal{T}(\boldsymbol{\xi}^{(m)})$. The leave-one-out (LOO) error ε_l of $\mathcal{T}(\boldsymbol{\xi}^{(m)})$ quantifies its accuracy as in

$$\varepsilon_l = \frac{1}{\mathcal{M}} \sum_{m=1}^{\mathcal{M}} \left(\frac{|\boldsymbol{E}_m|^2 - \mathcal{T}(\boldsymbol{\xi}^{(m)})}{1 - h_m} \right)^2, \tag{11}$$

where h_m is the m-th diagonal element of the square matrix $\hat{\boldsymbol{\Psi}}(\hat{\boldsymbol{\Psi}}^T\hat{\boldsymbol{\Psi}})^{-1}\hat{\boldsymbol{\Psi}}^T$. Note that we use $\mathcal{T}(\boldsymbol{\xi}^{(m)})$, not $\widehat{\mathcal{T}}(\boldsymbol{\xi}^{(m)})$, to calculate ε_l. They have different meanings in the LARS method. $\widehat{\mathcal{T}}(\boldsymbol{\xi}^{(m)})$ enables us to select a set of predictors out of the $\mathcal{L}$ predictors, whereas $\mathcal{T}(\boldsymbol{\xi}^{(m)})$ is used as the estimate of $|\boldsymbol{E}_m|^2$ for $1 \le m \le \mathcal{M}$.

We control the LARS procedure by setting a threshold named as target error ε_t and calculate ε_l after each LARS iteration, and then compare ε_l with ε_t. When ε_l is less than or equal to ε_t, the LARS procedure is terminated. The termination of the LARS procedure may happen before all ψ are selected.

D. The adaptive LARS method

1) The potential problems of the LARS method:

Comparing with other model selection methods such as the least absolute shrinkage and selection operator (LASSO) method [27], the LARS method is more stable and computationally efficient. Nevertheless, there are some factors that may negatively influence the performance of the LARS method with respect to the accuracy and the stability.

1) The LARS method fails to capture the relations between $\boldsymbol{\xi}^{(m)}$ and $\mathcal{T}(\boldsymbol{\xi}^{(m)})$.

When the number of input samples is limited, the LARS method may not be able to capture the relations between $\boldsymbol{\xi}^{(m)}$ and $\mathcal{T}(\boldsymbol{\xi}^{(m)})$. This phenomenon is called underfitting. When underfitting occurs, $\mathcal{T}(\boldsymbol{\xi}^{(m)})$ usually shows a low accuracy.

2) Some chosen samples negatively impact the accuracy of $\mathcal{T}(\boldsymbol{\xi}^{(m)})$.
It is possible that some chosen $\boldsymbol{\xi}$ yields values of $|\boldsymbol{E}|^2$ which are substantially larger or smaller than the $|\boldsymbol{E}|^2$ values corresponding to all other $\boldsymbol{\xi}$. This sort of $|\boldsymbol{E}|^2$ is called an outlier which may negatively impact the accuracy of $\mathcal{T}(\boldsymbol{\xi}^{(m)})$.
3) Unreasonable setting of ε_t.
In the LARS method, we calculate ε_l in (11) after each LARS iteration and stop the LARS procedure when ε_l is less than ε_t or the number of LARS iterations equals $\mathcal{L}$. The setting of ε_t exerts a crucial influence on the final result of LARS method. An unreasonable setting of ε_t may cause unsatisfactory results. When ε_l is higher than ε_t throughout all the LARS iterations, the LARS procedure does not stop until all $\psi_{\boldsymbol{\alpha}_l}$ are incorporated into $\mathcal{Q}$. In such cases, the optimal result, which is most close to the result of MCM, may have already appeared in the earlier LARS iterations. However, due to the high value of ε_l, the LARS procedure does not stop at this iteration. Similarly, it is possible that the LARS procedure stops too early when ε_l is less than ε_t after a few number of LARS iterations. As a result, only a limited number of $\psi_{\boldsymbol{\alpha}_l}$ participate in the calculation of $\mathcal{T}(\boldsymbol{\xi})$ and thus the estimated standard deviation becomes unreliable.
4) Lack of flexibility on the required number of input samples.
To successfully perform the matrix inversion in (10), the total number of the chosen a should not exceed $\mathcal{M}$. In the LARS method, $\mathcal{M}$ should satisfy $\mathcal{L} \leq \mathcal{M}$. Such a condition restricts the minimum number of input samples.

2) Methods to improve the LARS method:

Four techniques are proposed aiming to circumvent these obstacles. In this paper, the LARS method with these four techniques is called as the adaptive LARS method.

1) In the LARS method, we can observe the possible underfitting phenomenon by detecting the change of ε_l. If ε_l obtained at the w-th LARS iteration is higher than the $(w-1)$th ε_l, the underfitting situation might have occurred. We prevent underfitting by stopping the LARS procedure if ε_l of the w-th LARS iteration exceeds that of the $(w-1)$th LARS iteration by a certain threshold value and taking the chosen polynomial bases obtained at the $(w-1)$th LARS iteration as the final chosen polynomial bases.
2) We set the minimum number of the LARS iterations to prevent the LARS procedure from being terminated too early by
   a) Setting the maximum number of the LARS iterations to $\mathcal{L}$.
   b) Reducing ε_t by a certain percentage at each LARS iteration when ε_l is less than ε_t before ζ LARS iterations so as to continue the LARS procedure until at least ζ polynomial bases are included in $\mathcal{Q}$, where ζ is a certain number of the LARS iterations for $1 \leq \zeta < \mathcal{L}$.
3) In the LARS method, we obtain $\mathcal{M}$ $|\boldsymbol{E}|^2$ from the $\mathcal{M}$ FDTD simulations. The variance of the $\mathcal{M}$ $|\boldsymbol{E}|^2$ is called sample variance. Since the LHS method has the property of spreading the sample points evenly across all possible values, it is likely that the sample variance obtained by LHS method is able to reflect the population variance to a certain degree [28]. We make use of this feature as an auxiliary condition to help us optimise the LARS result by taking the following steps.
   a) Calculate the sample variance $\hat{\sigma}^{\,2}$ of $\mathcal{M}$ $|\boldsymbol{E}|^2$ in
   $$\hat{\sigma}^{\,2} = \frac{1}{\mathcal{M}-1}\sum_{m=1}^{\mathcal{M}}\left(|\boldsymbol{E}_m|^2 - \frac{1}{\mathcal{M}}\sum_{i=1}^{\mathcal{M}}|\boldsymbol{E}_i|^2\right)^2. \quad (12)$$
   b) Calculate ε_l at each LARS iteration. When ε_l is less than ε_t and the number of LARS iterations is larger than ζ and less than ς , we run further ι LARS iterations instead of stopping LARS procedure, where $\iota \leq (\mathcal{L}-\varsigma)$ and $\zeta < \varsigma < \mathcal{L}$. When $\varepsilon_l \leq \varepsilon_t$, the variance $\left(\sigma^{(\mathcal{M})}\right)^2$ is calculated by
   $$\left(\sigma^{(\mathcal{M})}\right)^2 = \left\{\sum_{\mathcal{Q}} a_{\boldsymbol{\alpha}_l}{}^2, 1 \leq l \leq \mathcal{L}\right\} \quad (13)$$
   at the end of each LARS iteration.
   c) Compare the sample variance in (12) with the variance calculated at each LARS iteration in (13). We consider $\left(\sigma^{(\mathcal{M})}\right)^2$ closest to $\hat{\sigma}^{\,2}$ as the final result.
4) The restriction of $\mathcal{L} \leq \mathcal{M}$ is lifted by applying the L2 regularisation scheme to the LARS method. This enables the LARS method to get a reasonable pseudoinverse by introducing a regularisation factor ϱ into (10). Therefore, when the number of the chosen a is larger than $\mathcal{M}$, we calculate $A_{\mathcal{A}}$ by
   $$A_{\mathcal{A}} = \left(1_{\mathcal{A}}^T \hat{\boldsymbol{\Psi}}^T \hat{\boldsymbol{\Psi}} 1_{\mathcal{A}} + 1_{\mathcal{A}}^T \varrho 1_{\mathcal{A}}\right)^{-\frac{1}{2}}. \quad (14)$$
   With the L2 regularisation scheme, the LARS method is capable of functioning even when $\mathcal{M} < \mathcal{L}$. Such feature of the L2 regularisation scheme is used to identify the optimal value of $\mathcal{M}$ by running the LARS method varying $\mathcal{M}$ from 1 to a certain number ($\leq \mathcal{L}$). $\mathcal{M}$ is determined when $\sigma^{(\mathcal{M})}$ in (13) reaches the stable status. When $\vartheta = \frac{\left|\sigma^{(\mathcal{M}-1)} - \sigma^{(\mathcal{M}-2)}\right|}{\sigma^{(\mathcal{M}-1)}}$ and $\vartheta^{\dagger} = \frac{\left|\sigma^{(\mathcal{M})} - \sigma^{(\mathcal{M}-1)}\right|}{\sigma^{(\mathcal{M})}}$ are less than a certain small value ϖ, $\sigma^{(\mathcal{M})}$ has no obvious change with the increase of $\mathcal{M}$, and thus $\sigma^{(\mathcal{M})}$ can be regarded as stable, and $\mathcal{M}$ at this point is regarded as the optimal.

The adaptive LARS method is summarised in Fig. 1.

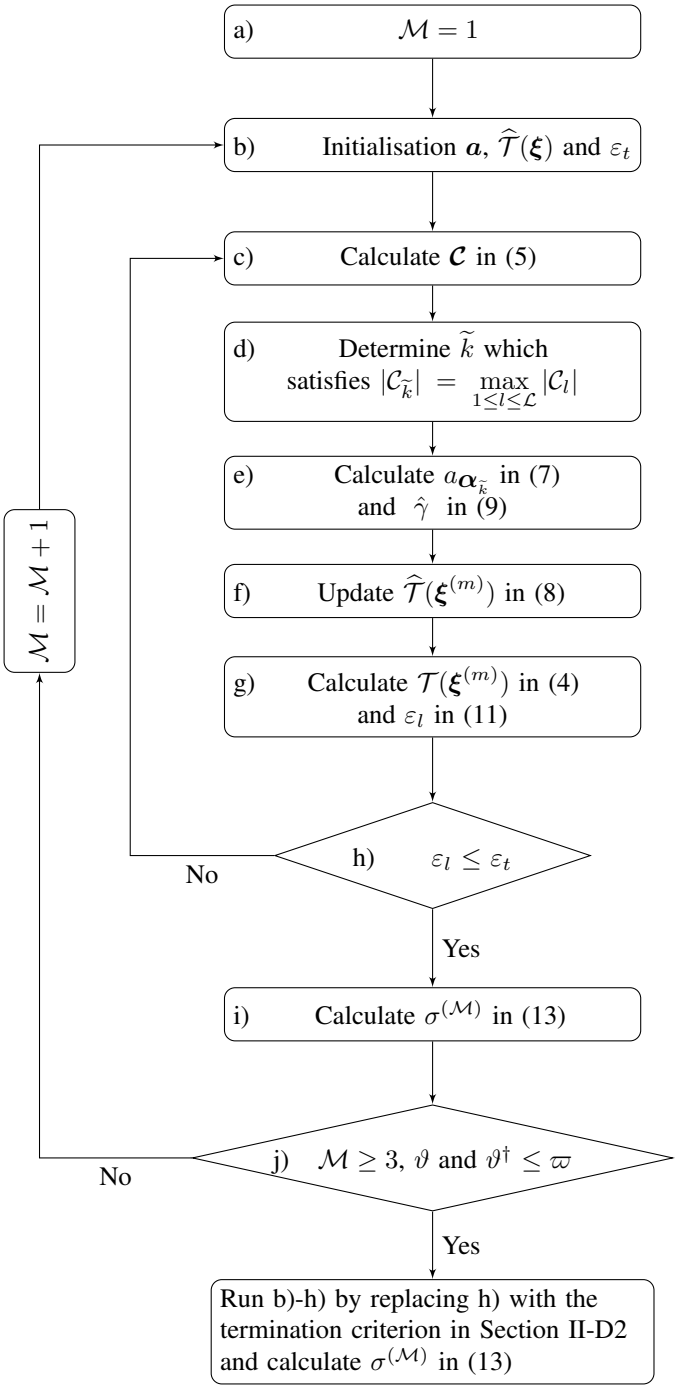

Fig. 1. The flow chart of the adaptive LARS method

III. NUMERICAL EXPERIMENTS SETTING FOR UNCERTAINTY QUANTIFICATION

The MCM, the LARS method and the adaptive LARS method are utilised to quantify the uncertainty of the FDTD results.

A. Radio environment setting

In the FDTD space, we place a point soft source excitation outside the human body and observe $\boldsymbol{E}$ in the middle of the prostate tissue. 10 layers of the complex frequency shifted-perfect matched layers (CFS-PML) [29] [30] are utilised to terminate the FDTD space. The DHP used in this work is 1mm spatial resolution and provided by RIKEN (Saitama, Japan) under the non-disclosure agreement between RIKEN and the University of Manchester. The usage was approved by RIKEN ethical committee.

This simulation scenario is depicted in Fig. 2. The excitation location is 17 mm away from the human body and the observation location is in the middle of the prostate tissue.

There are five influential tissues (fat, skin, muscle, bone and prostate) between the excitation and observation. $|\boldsymbol{E}|^2$ observed changes significantly when one or more of the Debye parameters of the influential tissues are changed. In the FDTD calculations, the relationship between $\boldsymbol{E}$ and the electric flux density $\boldsymbol{D}$ in one-pole Debye model is written as

$$\boldsymbol{D} = \epsilon_0 \left[\epsilon_\infty + \frac{\Delta\epsilon}{1+\jmath\omega\tau} + \frac{\kappa_S}{\jmath\omega\epsilon_0}\right]\boldsymbol{E}, \tag{15}$$

where ϵ_0 is the permittivity of a vacuum (8.8541×10^{-12} F/m), ω is the angular frequency, $\jmath$ is the imaginary unit satisfying $\jmath=\sqrt{-1}$, κ_S is the static conductivity, ϵ_∞ is the optical relative permittivity, ϵ_S is the static relative permittivity, τ is the relaxation time, and $\Delta\epsilon$ satisfies $\Delta\epsilon = \epsilon_S - \epsilon_\infty$. Each tissue in the DHP is associated with four Debye parameters $(\kappa_S, \epsilon_\infty, \Delta\epsilon, \tau)$. The Debye parameters for all human tissues are presented in [31]. The ϵ_∞ and $\Delta\epsilon$ are the influential Debye parameters for the five influential tissues.

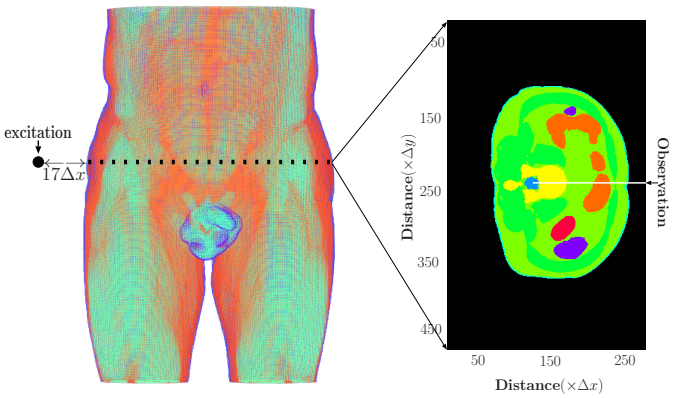

Fig. 2. Numerical simulation setup.

B. Numerical experiments for uncertainty quantification

1) The Monte Carlo method

a) Generate the 10^4 random ϵ_∞ and $\Delta\epsilon$ for each of 5 influential tissues yielding the normal distribution. In our scenario, 10^4 input samples enable the MCM method to reach convergence. $\mathcal{K}(=10)$ variables and their average and the corresponding standard deviation are listed in Table III. When we generate 10^4 samples for each variable, the relative permittivity and the conductivity of each tissue vary within ±10 percent.

b) Randomly pick one sample out of 10^4 samples for each variable and combine these chosen samples

ξ	Meaning of ξ	Average	Standard deviation
ξ_1	ϵ_∞ of fat	6.80	0.68
ξ_2	$\Delta\epsilon$ of fat	7.37	0.74
ξ_3	ϵ_∞ of skin	18.07	1.81
ξ_4	$\Delta\epsilon$ of skin	29.87	2.99
ξ_5	ϵ_∞ of muscle	28.93	2.88
ξ_6	$\Delta\epsilon$ of muscle	28.02	2.81
ξ_7	ϵ_∞ of bone	1.53	0.15
ξ_8	$\Delta\epsilon$ of bone	4.01	0.40
ξ_9	ϵ_∞ of prostate	32.82	3.28
ξ_{10}	$\Delta\epsilon$ of prostate	27.73	2.78

TABLE III
THE AVERAGE VALUES AND STANDARD DEVIATIONS OF THE 10 VARIABLES AND THEIR CORRESPONDING NOTATION

to produce 1 combination of the 10 variables as in $\boldsymbol{\xi} = \{\xi_1, \xi_2, \cdots, \xi_{10}\}$.

c) Repeat Step 1b 10^4 times to produce 10^4 $\boldsymbol{\xi}$. In Step 1b, we do not choose the same samples as those chosen earlier.

d) Run 10^4 FDTD simulations each with a different $\boldsymbol{\xi}$ to obtain 10^4 $|\boldsymbol{E}|^2$.

e) Calculate

$$\nu(\mathcal{M}) = \frac{1}{\mathcal{M}} \sum_{m=1}^{\mathcal{M}} |\boldsymbol{E}_m|^2 \tag{16}$$

and

$$\sigma(\mathcal{M})^2 = \frac{1}{\mathcal{M}-1} \sum_{m=1}^{\mathcal{M}} (|\boldsymbol{E}_m|^2 - \nu(\mathcal{M}))^2 \tag{17}$$

of the first $\mathcal{M}$ $|\boldsymbol{E}|^2$ among the 10^4 $|\boldsymbol{E}|^2$ varying $\mathcal{M}$ from 2 to 10^4

2) The LARS method

In the LARS method, the setting of ε_t is crucial. Empirically, $\varepsilon_t = 10^{-3}$ is a reasonable value in our scenario enabling the LARS method to have a stable performance. Fig. 3 and Fig. 4 show the $\sigma^{(\mathcal{M})}$ and the ε_l varying LARS iterations respectively in case when $q = 0.4$, $\mathcal{K} = 10$, $\mathcal{M} = 20$ and $\mathcal{L} = 20$. The ε_l is less than ε_t at the 14th LARS iteration and the LARS procedure is therefore terminated at the 14th iteration. Thus, there are 14 $a_{\boldsymbol{\alpha}_l}\psi_{\boldsymbol{\alpha}_l}$ in total in $\mathcal{Q}$, in the order of $l = \{6, 14, 7, 3, 1, 2, 20, 11, 13, 9, 4, 8, 12, 19\}$.

We set ϱ in (14) to 10^{-8} in order to obtain an accurate pseudoinverse. In the case of 10 Debye parameters of interest as shown in Table III, $\sigma^{(\mathcal{M})}$ is calculated in (13) when $q = 0.4$, $r = 2$, and $\varepsilon_t = 10^{-3}$.

3) The adaptive LARS method

The same parameters as the LARS method are used for the adaptive LARS method. In the adaptive LARS method, the LARS method is run first to determine the optimal value of $\mathcal{M}$. We determine the optimal $\mathcal{M}$ under the condition that ϑ and $\vartheta^\dagger$ are less than ϖ. The setting of ϖ is application-specific. In our scenario, ϖ of 0.03 enables us to identify the stable $\sigma^{(\mathcal{M})}$. The condition of ϑ and $\vartheta^\dagger$ less than 0.03 is satisfied when $\mathcal{M} = 15$.

Fig. 5 shows $\sigma^{(\mathcal{M})}$ varying $\mathcal{M}$ from 1 to $20(= \mathcal{L})$. $\sigma(10^4)$ in (17) from 10^4 FDTD results in MCM is presented as a dashed line for comparison. The results of

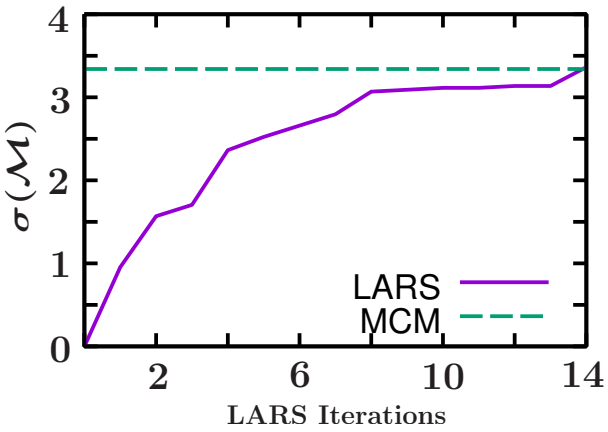

Fig. 3. $\sigma^{(\mathcal{M})}$ in (13) from the LARS method and $\sigma(10^4)$ in (17) from MCM is presented as a dashed line for comparison.

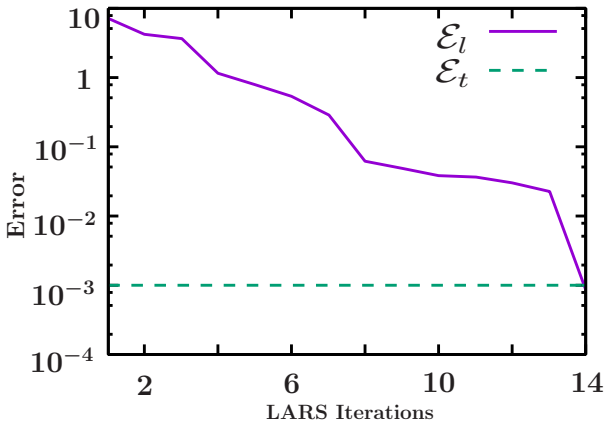

Fig. 4. The LOO error varying the LARS iterations.

$\sigma^{(\mathcal{M})}$ are neither stable nor accurate when $\mathcal{M} < 15$ and the accuracy of $\sigma^{(\mathcal{M})}$ shows no obvious improvement when $\mathcal{M} \geq 15$. This proves that $\mathcal{M} = 15$ is a optimal value in our scenario. We use 15 samples for UQ in the adaptive LARS methods leading to the adaptive LARS method which only requires 75% of the FDTD simulations needed by the original LARS method. We run the LARS iteration again with the determined $\mathcal{M}$ until one of the conditions which is described in Table IV is triggered. Table IV lists the conditions which may happen in the LARS procedure and the corresponding steps to calculate $\sigma^{(\mathcal{M})}$ of $|\boldsymbol{E}|^2$. Empirically, we set $\zeta = \frac{\mathcal{L}}{4}$, $\iota = \frac{5\mathcal{L}}{6}$, and $\varsigma = \frac{\mathcal{L}}{6}$.

The adaptive LARS method mainly focuses on determining $\sigma^{(\mathcal{M})}$. The calculation of ν is identical for both the adaptive LARS method and the LARS method. We calculate ν in (16) with the determined $\mathcal{M}$.

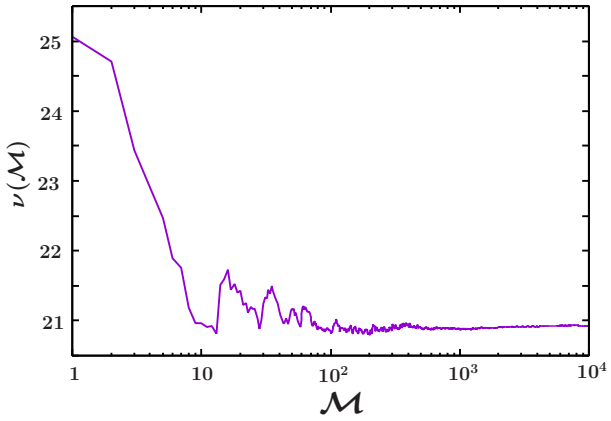

Fig. 6. $\nu(\mathcal{M})$ in (16) from MCM.

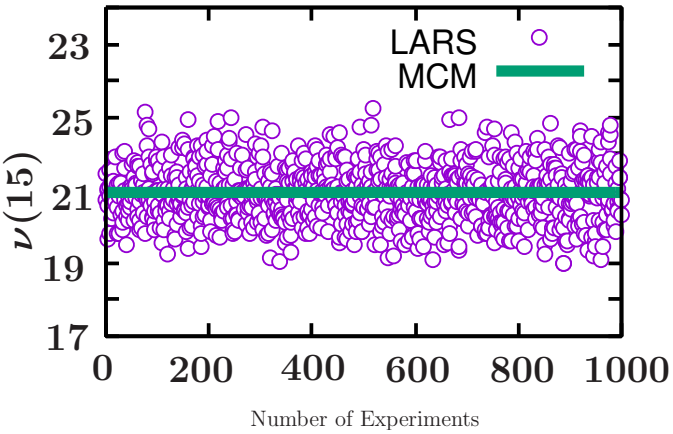

Fig. 7. 1000 $\nu(15)$ from the LARS method and $\nu(10^4)$ from MCM.

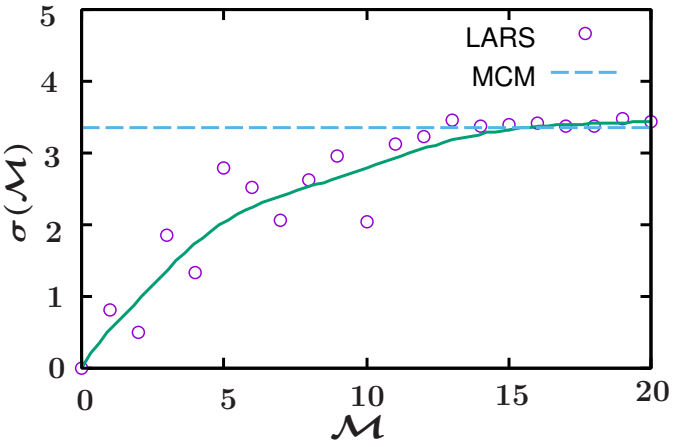

Fig. 5. $\sigma^{(\mathcal{M})}$ in (13) from the LARS method varying $\mathcal{M}$ from 0 to 20. $\sigma(10^4)$ in (17) from MCM is presented as a dashed line for comparison purpose.

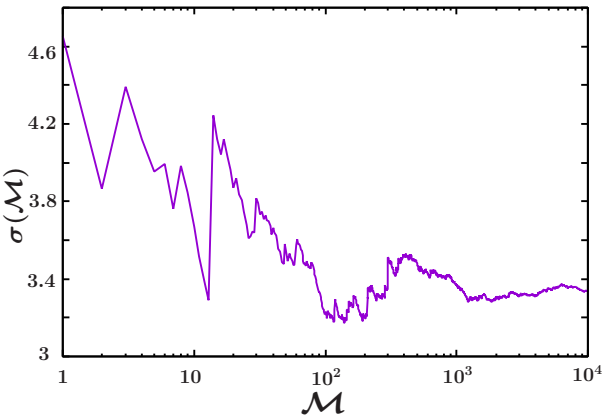

Fig. 8. $\sigma(\mathcal{M})$ in (17) from the MCM.

IV. Results and Discussions

We show ν and $\sigma^{(\mathcal{M})}$ obtained from the MCM, the LARS and the adaptive LARS methods. Some results obtained from the LARS method are not satisfactory. We present these results and their corresponding results obtained from the adaptive LARS method as a demonstration of the merit of the adaptive LARS method.

A. Results

1) Average values
The $\nu(\mathcal{M})$ of the first $\mathcal{M}$ $|\boldsymbol{E}|^2$ obtained from the MCM is presented in Fig. 6, where $\mathcal{M}$ varies from 2 to 10^4. Fig. 7 shows ν obtained from the LARS method when $\mathcal{M} = 15$, $\mathcal{K} = 10$ and $r = 2$. The $\nu(10^4)$ from the MCM is presented as a straight line for comparison.
2) Standard deviations
Fig. 8 is $\sigma(\mathcal{M})$ in (17) of the first $\mathcal{M}$ $|\boldsymbol{E}|^2$ obtained from the MCM, where $\mathcal{M}$ varies from 2 to 10^4.
Fig. 9 presents $\sigma^{(\mathcal{M})}$ obtained from the LARS method when $\mathcal{M} = 15$, $\mathcal{K} = 10$ and $r = 2$. $\sigma(10^4)$ from the MCM is presented as a straight line for comparison. We call the results of the LARS method more than $\pm$ 5% away from the result of MCM as unsatisfactory as shown in Fig. 10a. These unsatisfactory results are then improved by the adaptive LARS method as shown in Fig. 10b.

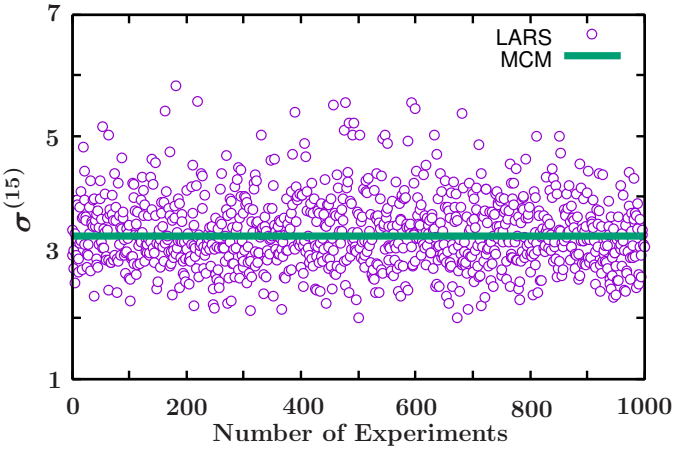

Fig. 9. 1000 $\sigma^{(15)}$ from the LARS method and $\sigma(10^4)$ in (17) from MCM.

Conditions	Steps to calculate $\sigma^{(\mathcal{M})}$
ε_l of the w-th LARS iteration is more than twice that of the $(w-1)$th LARS iteration.	a) Terminate LARS procedure. b) Calculate $\sigma^{(\mathcal{M})}$ in (13) using the elements in $\mathcal{Q}$ obtained at the $(w-1)$th LARS iteration.
$\varepsilon_l \leq \varepsilon_t$ before $\frac{\mathcal{L}}{4}$ LARS iterations.	a) Set ε_t to half of its originally set ε_t. b) Repeat Step 3a until at least $\frac{\mathcal{L}}{4}$ polynomial bases are included in $\mathcal{Q}$. c) Calculate $\sigma^{(\mathcal{M})}$ in (13) using the elements in $\mathcal{Q}$.
$\varepsilon_l \leq \varepsilon_t$ and the number of LARS iterations is larger than $\frac{\mathcal{L}}{4}$ and less than $\frac{5\mathcal{L}}{6}$.	a) Calculate $\hat{\sigma}^{\,2}$ of the 15 $\lvert\boldsymbol{E}\rvert^2$ in (12). b) Let the LARS procedure execute further $\frac{\mathcal{L}}{6}$ LARS iterations and calculate $\left(\sigma^{(\mathcal{M})}\right)^2$ in (13) whose corresponding ε_l is less than ε_t at each LARS iteration . c) Compare $\hat{\sigma}^{\,2}$ with the variance calculated at each LARS iteration and choose the closest $\left(\sigma^{(\mathcal{M})}\right)^2$ to the sample variance as the final result.
$\varepsilon_l \leq \varepsilon_t$ and the number of LARS iterations is larger than $\frac{5\mathcal{L}}{6}$ or equal to $\frac{5\mathcal{L}}{6}$.	Calculate $\sigma^{(\mathcal{M})}$ in (13) using the elements incorporated in $\mathcal{Q}$.
$\varepsilon_l > \varepsilon_t$ and the number of LARS iterations equals $\mathcal{L}$.	

TABLE IV
THE POSSIBLE CONDITIONS IN THE LARS PROCEDURE AND THE CORRESPONDING STEPS TO CALCULATE $\sigma^{(\mathcal{M})}$

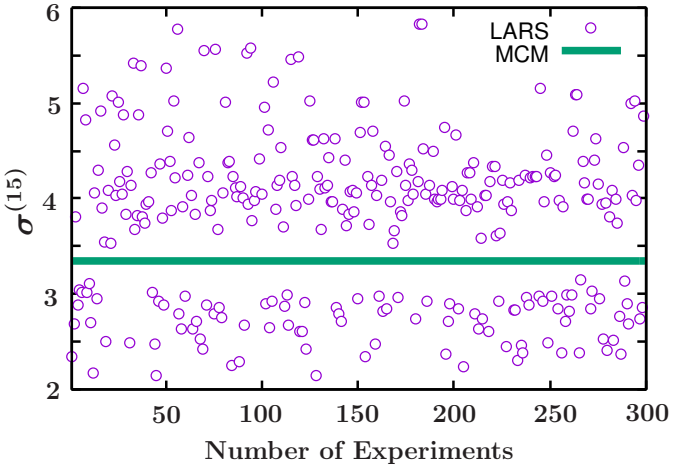

(a) 300 $\sigma^{(15)}$ from Fig. 9 more than $\pm 5\%$ of the $\sigma(10^4)$ of MCM.

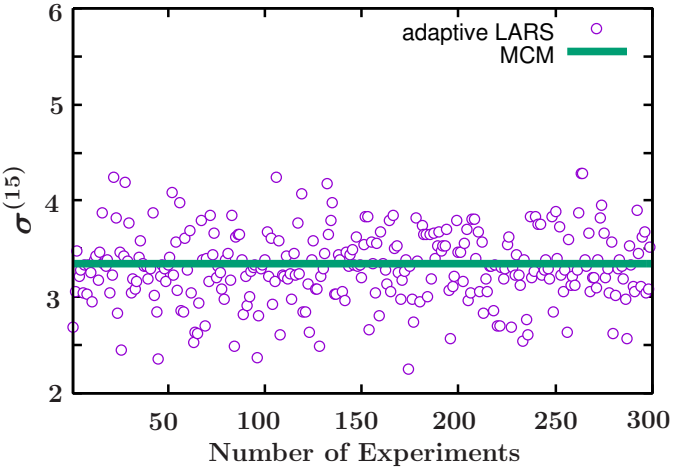

(b) $\sigma^{(15)}$ from the adaptive LARS method.

Fig. 10. (a) Unsatisfactory $\sigma^{(15)}$ obtained from the LARS method. (b) the corresponding $\sigma^{(15)}$ from the adaptive LARS method.

B. Discussions

300 $\sigma^{(15)}$ out of 1000 $\sigma^{(15)}$ in Fig. 9 are improved by the adaptive LARS method as shown in Fig. 10.

The numerical experiments for UQ involve 10 Debye parameters which can be expanded with 65 polynomial terms by the general full PC truncation scheme. By using the hyperbolic scheme, the number of polynomial terms is reduced from 65 to 20, and thus the required number of the FDTD simulations is reduced to 20 as well. By determination of the optimal value of $\mathcal{M}$ applying the L2 regularisation scheme, the number of the required FDTD simulations is further reduced to 15, thereby optimally reducing the computational cost. Although the process of determining $\mathcal{M}$ makes the adaptive LARS method more complex than the conventional LARS method, the computational cost of the entire process of the adaptive LARS method is still significantly lower than the conventional LARS method due to reduction of the required FDTD simulations and we achieve higher accuracy than the original LARS method.

V. CONCLUSIONS

The *curse of dimensionality* recurs in almost all UQ techniques in circumstances which involve a high number of input parameters. To overcome this problem, this paper introduced the hyperbolic scheme in the NIPC expansion to create a sparse NIPC expansion. The L2 regularisation scheme was applied to the LARS method to enable the matrix inversion to be performed irrespective of the number of samples. This allowed the LARS method to be successfully completed using only 15 FDTD simulations for 10 input variables, whereas the required number of FDTD simulations would be at least 65 in the conventional LARS method. As a consequence, the computational cost was only 23.1% of the general NIPC expansion. The proposed adaptive LARS method mainly focuses on the optimisation of the LARS method with respect to the accuracy. Its contribution lies in the analysis of the termination criterion of the LARS procedure. However, it also shows a better stability than the LARS method since it reduces the impact of the inadequate samples.

ACKNOWLEDGEMENT

This work was completed in part with HOKUSAI-GreatWave Computer System at RIKEN. http://i.riken.jp/download/sites/2/HOKUSAI_system_overview_en.pdf.

REFERENCES

[1] J. C. Liberti and T. S. Rappaport, *Smart antennas for wireless communications: IS-95 and third generation CDMA applications*. Prentice Hall PTR, 1999.

[2] K. Sairam, N. Gunasekaran, and S. R. Redd, "Bluetooth in wireless communication," *IEEE Commun. Mag.*, vol. 40, no. 6, pp. 90–96, 2002.

[3] S. Rathod, "Investigation of electromagnetic radiations in mumbai," *IETE Journal of Education*, vol. 55, no. 2, pp. 81–89, 2014.

[4] M. A. Esmekaya, C. Ozer, and N. Seyhan, "900 MHz pulse-modulated radiofrequency radiation induces oxidative stress on heart, lung, testis and liver tissues," *Gen Physiol. Biophys.*, vol. 30, no. 1, pp. 84–89, 2011.

[5] J. C. Lin, "The blood-brain barrier, cancer, cell phones, and microwave radiation," *IEEE Antennas Propag. Mag.*, vol. 43, no. 3, pp. 141–143, 2001.

[6] J. Wiart, A. Hadjem, M. Wong, and I. Bloch, "Analysis of rf exposure in the head tissues of children and adults," *Physics in Medicine & Biology*, vol. 53, no. 13, p. 3681, 2008.

[7] M.-C. Gosselin, A. Christ, S. Kühn, and N. Kuster, "Dependence of the occupational exposure to mobile phone base stations on the properties of the antenna and the human body," *IEEE Trans. Electromagn. Compat.*, vol. 51, no. 2, pp. 227–235, 2009.

[8] A. Taflove and S. C. Hagness, *Computational electrodynamics: the finite-difference time-domain method*. Artech house, 2005.

[9] K. Yee, "Numerical solution of initial boundary value problems involving maxwell's equations in isotropic media," *IEEE Trans. Antennas Propag.*, vol. 14, no. 3, pp. 302–307, 1966.

[10] P. Kosmas and C. M. Rappaport, "Time reversal with the fdtd method for microwave breast cancer detection," *IEEE Trans. Microw. Theory and Tech.*, vol. 53, no. 7, pp. 2317–2323, 2005.

[11] K. Tekbas, F. Costen, R. Himeno, and J.-P. Berenger, "Subcell modelling of frequency dependent thin layers in the fdtd method," *IEEE Trans. Antennas Propag.*, vol. 65, no. 4, pp. 1321–1329, 2017.

[12] N. R. Mehrabadi, R. Burgos, C. Roy, and D. Boroyevich, "Power electronics modeling and design: Using parametric and model-form uncertainty quantification to assess predictive accuracy of power converter models," *IEEE Power Electron. Mag.*, vol. 4, no. 4, pp. 44–52, 2017.

[13] A. Arduino, M. Chiampi, F. Pennecchi, L. Zilberti, and O. Bottauscio, "Monte carlo method for uncertainty propagation in magnetic resonance-based electric properties tomography," *IEEE Trans. Magn.*, vol. 53, no. 11, pp. 1–4, 2017.

[14] C. Yardim, P. Gerstoft, and W. S. Hodgkiss, "Estimation of radio refractivity from radar clutter using bayesian monte carlo analysis," *IEEE Trans. Antennas Propag.*, vol. 54, no. 4, pp. 1318–1327, 2006.

[15] Y. Chen, J. Wen, and S. Cheng, "Probabilistic load flow method based on nataf transformation and latin hypercube sampling," *IEEE Trans. Sustainable Enery.*, vol. 4, no. 2, pp. 294–301, 2013.

[16] R. B. Thakur, Q. Y. Tang, R. McGeehan, F. Carter, and E. Shirokoff, "Characterizing quality factor of niobium resonators using a markov chain monte carlo approach," *IEEE Trans. Appl. Supercond.*, vol. 27, no. 4, pp. 1–5, 2017.

[17] H. Acikgoz and R. Mittra, "Stochastic polynomial chaos expansion analysis of a split-ring resonator at terahertz frequencies," *IEEE Trans. Antennas Propag.*, vol. 66, no. 4, pp. 2131–2134, 2018.

[18] X. Cheng and V. Monebhurrun, "Application of different methods to quantify uncertainty in specific absorption rate calculation using a cad-based mobile phone model," *IEEE Trans. Electromagn. Compat.*, vol. 59, no. 1, pp. 14–23, 2017.

[19] K. Li, T.-Z. Huang, L. Li, S. Lanteri, L. Xu, and B. Li, "A reduced-order discontinuous galerkin method based on pod for electromagnetic simulation," *IEEE Trans. Antennas Propag.*, vol. 66, no. 1, pp. 242–254, 2018.

[20] I. Jeong, B.-G. Gu, J. Kim, K. Nam, and Y. Kim, "Inductance estimation of electrically excited synchronous motor via polynomial approximations by least square method," *IEEE Trans. Ind. Appl.*, vol. 51, no. 2, pp. 1526–1537, 2015.

[21] G. Blatman and B. Sudret, "Adaptive sparse polynomial chaos expansion based on least angle regression," *Journal of Computational Physics*, vol. 230, no. 6, pp. 2345–2367, 2011.

[22] G. E. Box, J. S. Hunter, and W. G. Hunter, *Statistics for experimenters: design, innovation, and discovery*, vol. 2. Wiley-Interscience New York, 2005.

[23] B. Efron, T. Hastie, I. Johnstone, and R. Tibshirani, "Least angle regression," *The Annals of statistics*, vol. 32, no. 2, pp. 407–499, 2004.

[24] P.-Y. Wu, C.-C. Fang, J. M. Chang, and S.-Y. Kung, "Cost-effective kernel ridge regression implementation for keystroke-based active authentication system," *IEEE Trans. Cybern.*, vol. 47, no. 11, pp. 3916–3927, 2017.

[25] C. Soize and R. Ghanem, "Physical systems with random uncertainties: chaos representations with arbitrary probability measure," *SIAM Journal on Scientific Computing*, vol. 26, no. 2, pp. 395–410, 2004.

[26] A. M. Molinaro, R. Simon, and R. M. Pfeiffer, "Prediction error estimation: a comparison of resampling methods," *Bioinformatics*, vol. 21, no. 15, pp. 3301–3307, 2005.

[27] L. Lian, A. Liu, and V. K. Lau, "Weighted lasso for sparse recovery with statistical prior support information," *IEEE Trans. Signal Process.*, 2018.

[28] J. F. Kenney, *Mathematics of statistics*. D. Van Nostrand Company Inc; Toronto; Princeton; New Jersey; London; New York,; Affiliated East-West Press Pvt-Ltd; New Delhi, 2013.

[29] J.-P. Berenger, "A perfectly matched layer for the absorption of electromagnetic waves," *Journal of computational physics*, vol. 114, no. 2, pp. 185–200, 1994.

[30] S. D. Gedney, G. Liu, J. A. Roden, and A. Zhu, "Perfectly matched layer media with cfs for an unconditionally stable adi-fdtd method," *IEEE Trans. Antennas Propag.*, vol. 49, no. 11, pp. 1554–1559, 2001.

[31] "The RIKEN webpage, media parameters for the Debye relaxation model," http://cfd-duo.riken.jp/cbms-mp/. Accessed: Oct. 3, 2017.

APPENDIX A
MATHEMATICAL NOTATIONS

ψ	Polynomial basis
r	Order of NIPC expansion
$\mathcal{K}$	Number of Debye parameters of interest
ξ	Debye parameters of interest
α	Index of polynomial basis
$\boldsymbol{\alpha}$	Collective form of $\alpha_1\alpha_2\cdots\alpha_\mathcal{K}$
$\mathcal{L}$	Number of polynomial bases in the NIPC expansion
$\mathcal{M}$	Number of samples
$\mathcal{T}(\boldsymbol{\xi}^{(m)})$	Predicted value of $\lvert\boldsymbol{E}\rvert^2$ for $\boldsymbol{\xi}^{(m)}$
$\widehat{\mathcal{T}}(\boldsymbol{\xi}^{(m)})$	Current LARS update of $\mathcal{T}(\boldsymbol{\xi}^{(m)})$
a	Coefficient of ψ
$\mathcal{C}$	Correlation between ψ and the residual vector
$\boldsymbol{\mathcal{E}}$	Vector of $\mathcal{M}$ $\lvert\boldsymbol{E}\rvert^2$
$\hat{\boldsymbol{\Psi}}$	Matrix of the chosen ψ
$\hat{\boldsymbol{a}}$	Vector of the coefficients of the chosen ψ
$\widetilde{k}$	Index of the most correlated polynomial basis
$\mathcal{Q}$	A set containing the chosen $a_{\boldsymbol{\alpha}_{\widetilde{k}}}\psi_{\boldsymbol{\alpha}_{\widetilde{k}}}$
$\hat{\gamma}$	Update coefficient of the LARS method
w	Index of LARS iteration
ε_t	Target error
ε_l	LOO error
ϱ	Regularisation factor
ζ	Minimum number of polynomial bases in $\mathcal{Q}$
ι	Number of additional LARS iterations
ς	Intermediate upperlimit of the number of LARS iterations
$\nu(\mathcal{M})$	Average value from the MCM
$\sigma(\mathcal{M})$	Standard deviation from the MCM
$\sigma^{(\mathcal{M})}$	Standard deviation from the LARS and adaptive LARS methods with $\mathcal{M}$ samples

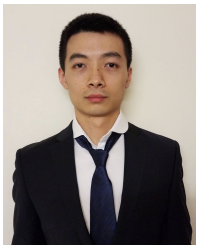

Runze Hu received the B.S. degree in computer science from the North China Electric Power University, Baoding, China, in 2014, and the M.Sc. degree in computer science from the University of Manchester, Manchester, U.K., in 2016. He started his Ph.D. study in Electrical and Electronics Engineering, University of Manchester, U.K., in 2017. His current research interests include artificial intelligence, uncertainty quantification techniques, and high-performance computing.

Fumie Costen (M'07) received the B.Sc. degree, the M.Sc. degree in electrical engineering and the Ph.D. degree in Informatics, all from Kyoto University, Japan. From 1993 to 1997 she was with Advanced Telecommunication Research International, Kyoto, where she was engaged in research on direction-of-arrival estimation based on Multiple SIgnal Classification algorithm for 3-D laser microvision. She filed three patents from the research in 1999 in Japan. She was invited to give 5 talks in Sweden and Japan during 1996-2014. From 1998 to 2000, she was with Manchester Computing in the University of Manchester, U.K., where she was engaged in research on metacomputing and has been a Lecturer since 2000. Her research interests include computational electromagnetics for microwave frequency range, microwave imaging, uncertainty quantification, and machine learning. She filed a patent from the research on the boundary conditions in 2012 in the U.S.A. Her work extends to the hardware acceleration of the computation using general-purpose computing on graphics processing units, Streaming Single Instruction Multiple Data Extension and Advanced Vector eXtentions instructions. Dr. Costen received an ATR Excellence in Research Award in 1996 and a best paper award from 8th International Conference on High Performance Computing and Networking Europe in 2000.

Hideo Yokota received his Doctor of Engineering degree from the University of Tokyo in 1999. In 1993, he joined Higuchi Ultimate Mechatronics Project, Kanagawa Academy of Science and Technology, Kawasaki, Japan. In 1999, he joined RIKEN and is the contract researcher of Computational biomechanics unit. 2004-2012 Bio-research Infrastructure Construction Team Leader, VCAD system research program, RIKEN. 2007-2012 Cell-scale Research and Development Team Leader,Research Program for Computational Science, RIKEN. 2013-present Image Processing Research Team Leader, Center for Advanced Photonics,RIKEN. He is also a visiting Professor at Hokkaido University, Kobe University, Tokai University and the Tokyo University of Agriculture and Technology. He currently studies biomedical imaging and image processing to the biomedical simulation. Bioimaging Society, Best Image Award, 2005. The Commendation for Science and Technology by the Minister of Education, Culture, Sports, Science and Technology , Young Scientists Prize in 2008.

Vikass Monebhurrun (SM'07) received the PhD degree in electronics in 1994 and the Habilitation a Diriger des Recherches (HDR) in physics in 2010 from University Pierre et Marie Curie (Paris VI) and University Paris-Sud (Paris XI), respectively. He was engaged in research on electromagnetic non-destructive testing for nuclear power and aeronautical applications until 1998, following which he joined the Department of Electromagnetics at Supelec (CentraleSupelec since 2015). His research interests encompass time domain numerical modeling as well as radio frequency measurements. He actively participated in French National Research Programs on electromagnetic dosimetry since 1998, namely COMOBIO (1999-2002 on 2G systems), ADONIS (2003-2005 on 3G systems) and MULTIPASS (2007-2010 on 4G systems). His research contributed to international standardization committees of CENELEC, IEC, and IEEE. He is author and co-author of more than 100 peer-reviewed international conference and journal papers. He also holds three international patents on antennas for mobile communications. He is an active contributor to international standardization committees of IEC 62209, IEC 62232, IEC/IEEE 62704 and IEEE1528. He is currently a member of the European COST Action BM 1309. Dr. Monebhurrun serves as member of the Editorial Board of the IEEE COMPUMAG and IEEE CEFC conferences, and IEEE Transactions on Magnetics special issues since 1998. He is the founder of the IEEE Radio and Antenna Days of the Indian Ocean (RADIO) international conference and he served as General Chair for all six editions since 2012. In 2013, he initiated the Radio Society (Mauritius) for which he serves as President. He is currently the Chair of the international committees of IEC/IEEE 62704-3 and IEEE Antennas and Propagation Standards. He serves as Associate-Editor for the IEEE Antennas and Propagation Transactions and Magazine, and Editor of the IoP Conference Series: Materials Science and Engineering. He was the recipient of the Union Radio-Scientifique Internationale (URSI) Young Scientist Award in 1996. Two of his PhD students received Best Student Paper Awards at the BioEM 2014 international conference. Following the publication of the dual/logo IEC/IEEE 62704-3 international standard on computational dosimetry in 2017, he was awarded the IEEE Standards Association International Working Group Chair Award. He was recipient of the IEC 1906 Award in 2018.

Ryutaro Himeno received his Doctor of Engineering degree from the University of Tokyo in 1988. In 1979, he joined Nissan Motor Co., Ltd., where he has been engaged in the research of applying Computational Fluid Dynamics analysis to the car aerodynamic development. In 1998, he joined RIKEN. He is now a unit leader of Computational Engineering Applications Unit and a coordinator of Research and Development Group, Head Office for Information Systems and Cybersecurity. He is also a visiting Professor at Hokkaido University, Chiba University, Tokyo University of Science, Tokyo Denki University and University of Aizu. He currently studies Computational Bioengineering and High Performance Computing. He was a winner of 2006 Gordon Bell Prize (Honorable Mention, Peak Performance) and Computer Visualization Contest in 2000 by Nikkei Science. He received both JSME Computational Mechanics Award and Computational Award by Japan Association of Computational Mechanics in 2011 as well as JSME Computational Mechanics Achievement Award in 1997.